Progress In Electromagnetics Research M, Vol. 105, 9–20, 2021

Ultra-Wideband RCS Reduction of Circular Polarization Slot Antenna Array Based on Polarization Conversion Structures and Frequency-Selective Rasorber

Yu-Xin Zhang[1], Yong-Ling Ban[1, *], and Chow-Yen-Desmond Sim[2]

Abstract—This paper proposes an absorption-transmission-absorption (A-T-A) type frequency-selective rasorber (FSR) with high selectivity that is loaded above a polarization conversion structure (PCS) and applied to a circular polarization (CP) slot antenna array for ultra-wideband radar cross section (RCS) reduction. Outside the operational frequency band (out-of-band) of the antenna, the energy of the incident electromagnetic (EM) wave is directly absorbed by the FSR, whereas from within the operational frequency band (in-band) of the antenna, the incident EM wave penetrates the FSR and irradiates it on the PCS placed on the lower layer of the FSR structure, which meets the phase cancellation condition and is diffused at the same time, thereby realizing the in-band RCS reduction. Due to the lower insertion loss in the passband, higher quality factor (Q value) in the transmission band, and wider absorption band, the proposed FSR can minimize the gain loss (only 0.2 dB) of the CP slot antenna array and widen the RCS reduction bandwidth to 135.5% (5–26 GHz). In addition, due to the central symmetry of the FSR and PCS structures, the CP slot antenna array has monostatic RCS reduction performance for both horizontally polarized (HP) and vertically polarized (VP) incoming waves.

1. INTRODUCTION

As the antenna is a key component of a wireless communication system, the ability for an antenna to achieve low scattering performance (in-band and out-of-band) while ensuring its good radiation performance is now a research hotspot. Furthermore, because CP antenna arrays are widely used in many communication systems (such as satellite navigation and radar system), it is of great value to study the broadband attenuation of its RCS as well.

Phase cancellation [1–6] is an effective method to reduce the RCS of the antenna in the operational band. In [7], a diffuse scattering structure was proposed, which satisfies the phase cancellation condition across a wide frequency band. However, in the antenna structure, because the thickness of the dielectric substrate of the sub-array unit is non-uniform, therefore, the flatness of the surface is undermined, which in turn will strengthen the edge scattering.In addition, the bottom of this structure is a metal ground, and when it is loaded above the antenna, it will hinder the antenna's radiation. To resolve the problem of antenna radiation, in [8], the artificial magnetic conductor (AMC) structure is placed around the antenna and above the metal ground. However, this method is mainly applied to reduce the RCS of the metal ground, instead of reducing the RCS of the antenna.

Frequency-selective rasorber (FSR) or frequency-selective absorber (FSA) is a common method to reduce the RCS of the antenna (out-of-band) [9–14]. However, the presently reported FSR or FSA

Received 12 July 2021, Accepted 13 September 2021, Scheduled 24 September 2021

* Corresponding author: Yong-Ling Ban (byl@uestc.edu.cn).

[1] School of Electronic Science and Engineering, University of Electronic Science and Technology of China, Chengdu 611731, China.

[2] Department of Electrical Engineering, Feng Chia University, 47025, Taiwan.

has the following disadvantages: (1) a larger insertion loss in the FSR passband (or known as the transmission band) [15]; (2) a narrower bandwidth for an absorption rate greater than 80% [16]; (3) a wider transition band (the quality factor Q is small) between the absorption band and the passband [17]. Although some other work, such as [11], is based on the hybrid metasurface to realize RCS reduction (for in-band and out-of-band), the antenna can only work in a single linear polarization state.

Based on the above analysis, an FSR is initially designed, and it is later loaded above a CP slot antenna array that has merged (or stacked) with a polarization conversion structures (PCS). By doing so, a CP slot antenna array can be realized with ultra-wideband RCS reduction of 135.5% (5–26 GHz). The advantages of the proposed FSR include low insertion loss (less than 0.3 dB) in the passband, high Q value (4.68), and broadband absorption performance (lower absorption bandwidth of 78% and upper absorption bandwidth of 58.7%). Notably, for ease of understanding the context of this paper, the "absorption band" refers to the frequency band where the absorption rate of FSR is greater than 80%; the "passband" refers to the frequency band where the S_{21} of FSR is greater than -0.3 dB; and the "transition band" refers to the frequency band between the passband and the absorption band.

2. OPERATION PRINCIPLE AND DESIGN METHOD

2.1. Operation Principle

The principle and breakdown diagram of the FSR and PCS to realize ultra-wideband RCS reduction for the CP slot antenna array is shown in Fig. 1. When the out-of-band EM wave is incident on the FSR, the EM wave interacts with the FSR and is absorbed, in which part of the incoming wave is directly absorbed by the frequency-selective absorber (FSA) on the upper layer, and part of the incoming wave (after passing through the FSA but is reflected by the frequency selective surface (FSS) on the lower layer) is also absorbed by the FSA. When the in-band EM wave is incident on the FSR, it will be transmitted to the PCS, and based on the principle of phase cancellation, this part of the transmitted wave will be further diffused and scattered, so as to achieve the in-band RCS reduction of the antenna. In addition, because the FSR and PCS are symmetrical with respect to its central position, the CP slot antenna array (after loaded with FSR and PCS) can achieve desirable RCS reduction for both horizontally polarized incident waves and vertically polarized incoming waves. In addition, across the in-band, because the proposed FSR has exhibited low insertion loss and the PCS can further enhance the CP performance, the loading of the proposed FSR and PCS will not affect the transmission and reception of the antenna.

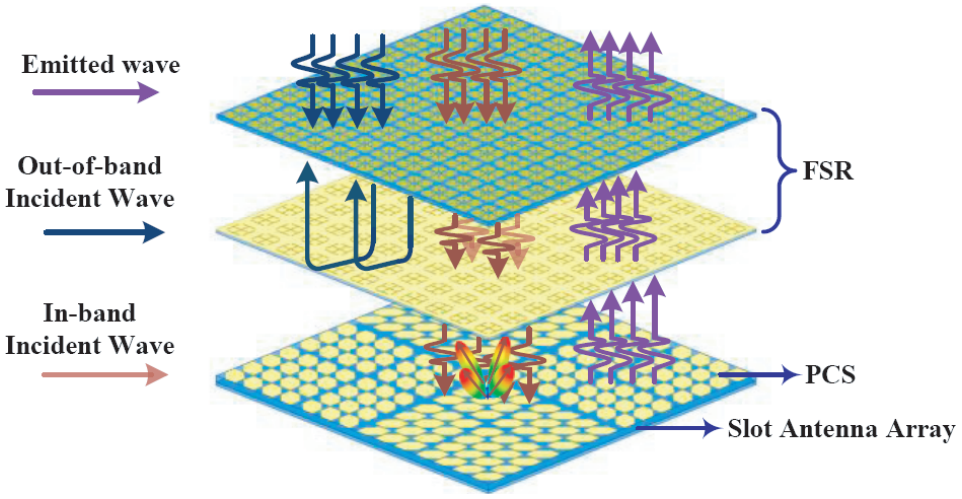

Figure 1. Operation principle and breakdown diagram of the CP slot antenna array loaded with FSR and PCS.

2.2. Design of FSR

The proposed FSR is composed of 11×11 periodic units, and the detailed geometry and structure of each FSR unit are depicted in Fig. 2. Here, the overall structure diagram of the FSR unit is as shown in Fig. 2(a), and it is composed of three different layers (upper, middle, and lower). The lower layer is a substrate of thickness $t_2 = 0.787\,\text{mm}$, and the FSS structure is printed on the top surface of this lower layer, as shown in Figs. 2(a) and 2(b). In the absorption band of FSR, the FSS is considered as a metal ground. In addition to reflecting the incoming wave (that transmits through the FSA) back to the FSA to be absorbed again, it is also possible to separate the FSA from the polarization conversion structure placed under the FSR to ensure that the impedance of the FSA is not affected by the polarization conversion structure, thereby ensuring the absorption characteristics of the FSR. Notably, the two substrates (upper and lower layers) are separated by an air gap (middle layer) of $h_1 = 4\,\text{mm}$. When the reflection coefficient of FSR is zero, the impedance of FSA is related to the air layer (see [18] for details). As for the upper layer that has a substrate thickness of $t_1 = 1.016\,\text{mm}$, it is also known as the FSA layer, because the passband FSA structure is printed on the two surfaces of this upper layer substrate, in which the top and bottom surfaces of the FSA structure are depicted in Figs. 2(c) and 2(d), respectively, and its corresponding design steps are shown in Fig. 3. As presented in Fig. 3, Step-I is to form an interdigital capacitance, thereby creating a passband in the absorption band of the FSA, and Step-II is to adjust the passband frequency of the FSA. It is noteworthy that all simulations were conducted using Ansoft High Frequency Structure Simulator (HFSS, version 19),

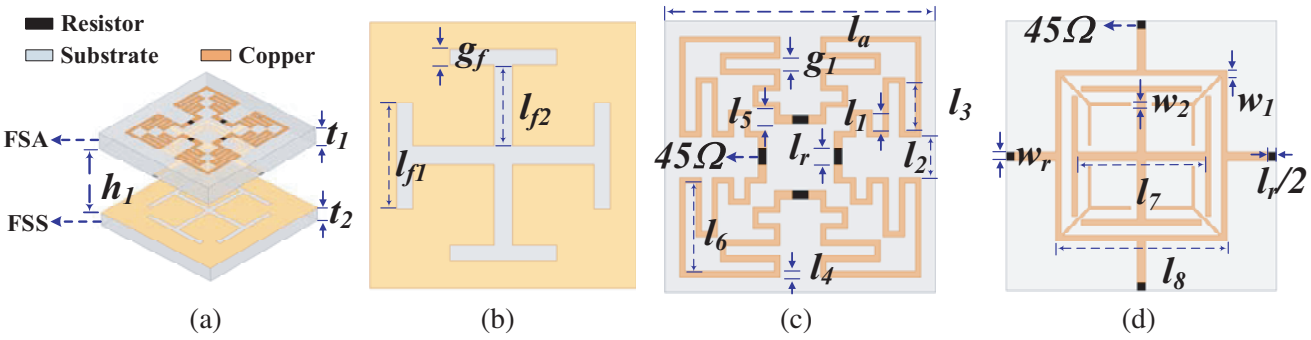

Figure 2. FSR structurer diagram and geometry. (a) Overall FSR unit composed of three different layers. (b) FSS printed on the upper surface of the lower layer. (c) Top surface structure of FSA (upper) layer with four resistors, each resistance is $45\,\Omega$. (d) Bottom surface structure of FSA (upper) layer with two resistors, each resistance is $90\,\Omega$. $t_1 = 1.016$, $t_2 = 0.787$, $h_1 = 4$, $l_2 = 1.1$, $l_a = 8$, $l_r = 0.3$, $l_{f1} = 3.9$, $l_{f2} = 2.25$, $l_1 = 0.6$, $l_2 = 0.3$, $l_3 = 1.2$, $l_4 = 0.2$, $l_5 = 0.5$, $l_6 = 2.74$, $l_7 = 2.74$, $l_8 = 3.74$, $w_r = 0.3$, $w_1 = 0.2$, $w_2 = 0.1$, $g_f = 0.3$, $g_1 = 0.1$. Unit: mm.

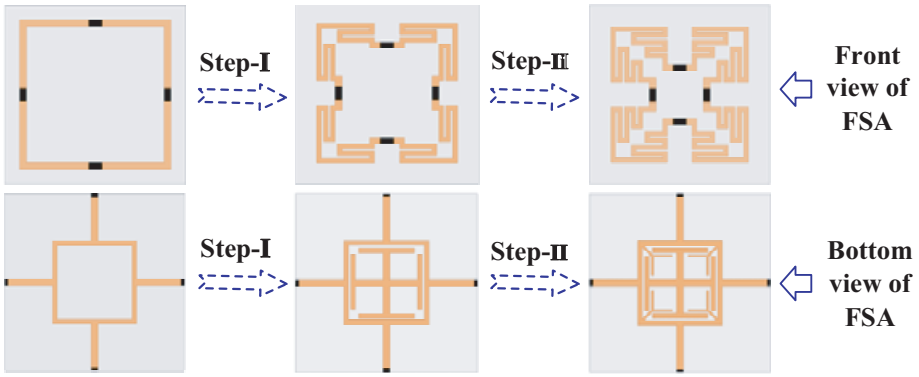

Figure 3. The design steps of achieving the proposed FSA.

and the calculation of the transmission coefficient of the FSR was done through periodic boundary conditions and Floquet port. Furthermore, the dielectric substrates used in the upper and lower layers of the FSR unit are Rogers 5880 (with dielectric constant 2.2 and loss angle 0.0009).

Figures 4(a) and 4(b) show the simulation method (model) and simulated results of the FSR, respectively, when the horizontally polarized (HP) and vertically polarized (VP) EM waves are incident normally. As can be seen from Fig. 4(b), the FSR maintains the same transmission characteristics for HP waves and VP waves when they are incident normally. Here, at out-of-band frequencies of 4.7–10.7 GHz and 13.25–24.25 GHz (with absorption bandwidth of 136%), the absorption rate of the FSR is greater than 80%. In the range of 11.8–12.08 GHz (which is the effective in-band of the antenna), the S_{21} (insertion loss) of the FSR is between −0.3 dB and −0.2 dB. The transition band (from passband to absorption band) is 10.7–11.8 GHz and 12.08–13.25 GHz, and the Q (quality factor) value is approximately 4.68.

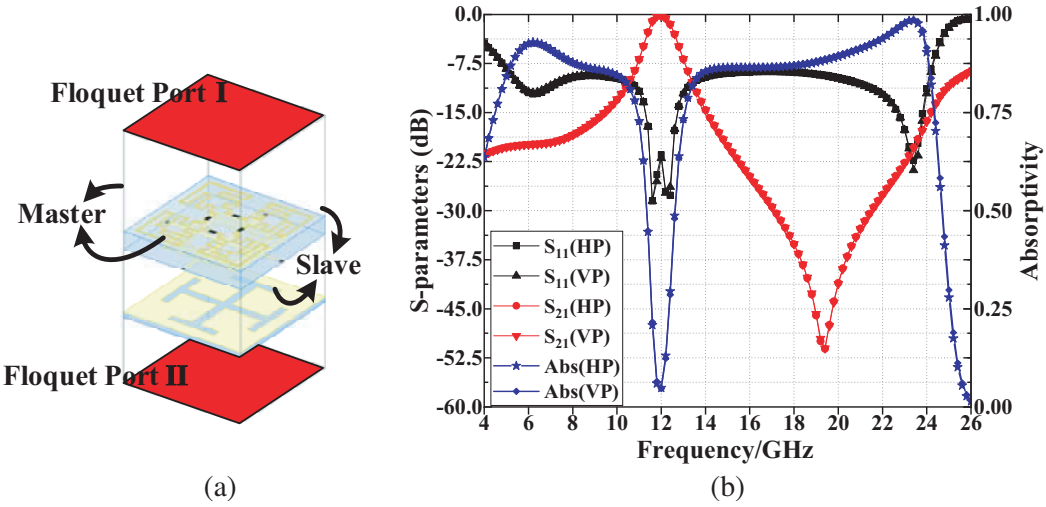

Figure 4. Simulation model and transmission characteristics of the FSR. (a) The simulation model of the FSR when the EM waves are incident vertically. (b) The transmission coefficient and absorption rate of FSR when the horizontal polarization (HP) and vertical polarization (VP) EM waves are normally incident.

Due to the central symmetry of the FSR structure (see Fig. 3) and the consistency of the transmission and absorption characteristics of the FSR when the vertically polarized EM wave and the horizontally polarized EM wave are incidents normally on the FSR, for brevity, only the transmission/reflection and absorption characteristics of the FSR (when horizontally polarized EM waves are incident obliquely) are discussed here, as shown in Fig. 5. In this figure, as the incident angle of EM waves increases, not only the passband frequency of the FSR does not vary, the insertion loss of the FSR in the passband has remained near constant as well. This indicates that the proposed FSR can be applied to a radome with wide-beam and wide-angle scanning antennas. Furthermore, the proposed FSR can be applied to the near field of these antennas, which is conducive to the low-profile design of the antenna. Notably, in the frequency band less than 21 GHz, as the S_{11} of the FSR increases slightly with the increase of the incident angle (of the incident wave), and the absorptivity (A) of the FSR is defined as below Eq. (1):

$$A = 1 - S_{11}^2 - S_{21}^2, \tag{1}$$

the absorption characteristic of the FSR has slightly deteriorated, but it can still maintain good absorption characteristics. As the frequency increases, the impedance of the FSR becomes sensitive to the angle of incidence (of the incident wave), in the range of 21–26 GHz, and the amplitude of the S_{11} is affected with multiple fluctuations. In view of the selected characteristics of the FSR, the sharp roll-off characteristic of the S_{21} in the transition zone does not vary with the incident angle (of the incident wave).

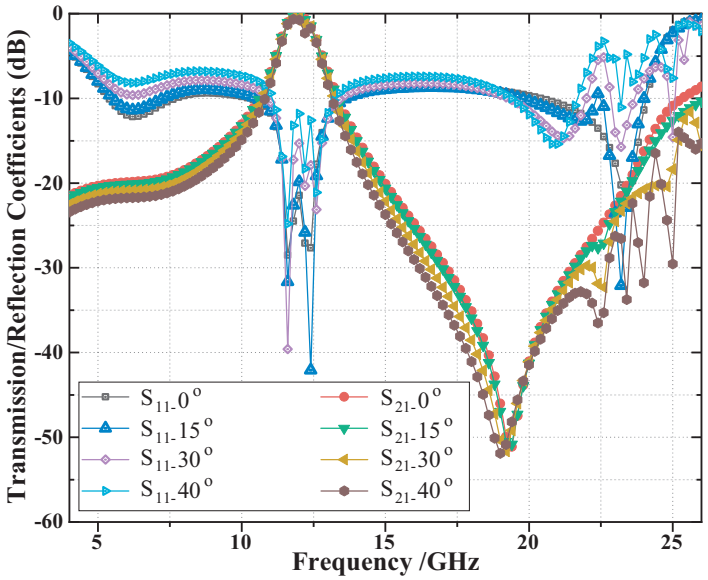

Figure 5. Simulation results of the FSR transmission/reflection characteristic curve at different incident angles.

2.3. The Design of PCS

The polarization conversion structure (PCS) is formed by using two types of structurer units (also known as polarization rotation reflection surface unit, PRRS unit), and they are shown in Fig. 6. The top views of the first unit cell type (Type 1) and second unit cell type (Type 2) that share the same planar size of $l_p \times l_p$ (5.6 mm × 5.6 mm) but with different truncated diagonal corners are depicted in Figs. 6(a) and 6(b), respectively. Notably, Type 2 is realized by rotating Type 1 (90° clockwise), and the overall 3-dimensional (3D) view of Type 1 is depicted in Fig. 6(c). Here, the dielectric substrate used by the unit cell is Rogers 5880 that has a planar size of $l_b \times l_b$ (6 mm × 6 mm) and a thickness of $t_{a2} = 1.575$ mm. As the principle of polarization rotation reflection surface (PRRS) is described in detail in [19], it will not be further discussed here.

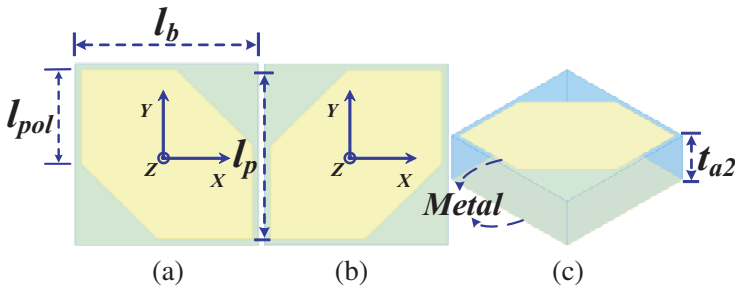

Figure 6. Geometry of the PCS structure unit cell (or PRRS unit cell). (a) Type 1. (b) Type 2. (c) The overall 3D view of Type 1. $l_b = 6$, $l_p = 5.6$, $l_{pol} = 3.1$, $t_{a2} = 1.575$. Unit: mm.

For the normal incidence of x- and y-polarized EM waves, the reflection coefficient of Type 1 is shown in Fig. 7. In this case, the reflected wave will have two components, the co-polarized (R_{xx} and R_{yy}) reflection component, and the cross-polarized (R_{yx} and R_{xy}) reflection component. As can be seen from Fig. 7, in the frequency range of 10.2–13.4 GHz, the PCS can fully reflect the incoming wave after polarization conversion, and for the two orthogonally polarized incoming waves, there is a 180°

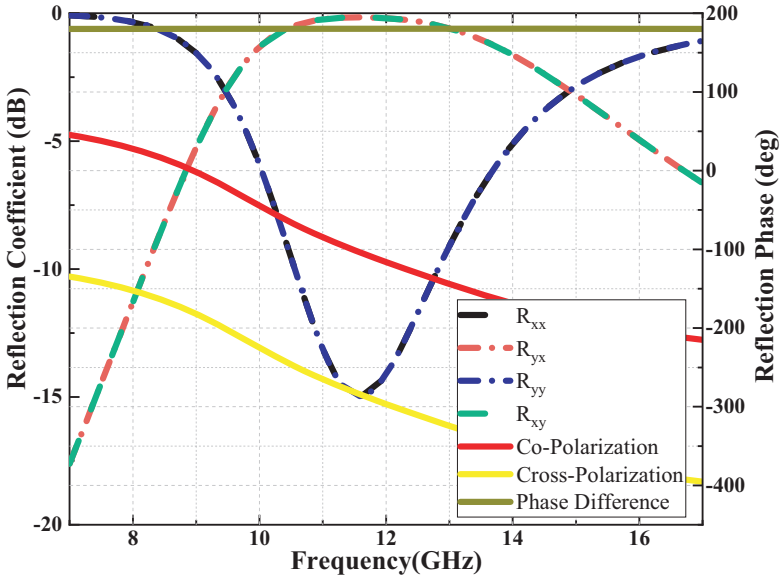

Figure 7. Simulated reflection coefficient amplitudes and reflection phase of Type 1.

reflection phase difference. By further studying Fig. 4 and Fig. 7, it can be found that the in-band of the PCS can cover the passband and the transition band of the FSR. This ensures that loading the FSR and PCS can achieve both the in-band RCS reduction of the CP slot antenna array and the out-of-band RCS reduction. As Type 2 has shown similar results as compared with Type 1, it is not discussed in here.

3. RESULTS AND DISCUSSION

Considering the size of the FSR units (FSA and FSS units) and PCS units, and also the convenience of validating the experiment results, the proposed FSR (formed by 11×11 units) and PCS (14×14 units) are devised and loaded onto the CP slot antenna array (formed by the 2×2 narrow rotational slots that are fed by the sequential rotational feeding network) which is shown in Fig. 8. Notably, one can expand the size of the CP slot antenna array (based on Fig. 8) to obtain greater gain. Part of the inner PCS unit (3×3 types) is shown in Fig. 8(a), and it can be seen that an L-shaped feeding line (narrow width of $w_s = 0.7\,\text{mm}$, vertical length of $l_{a2} + l_{a3}$, and horizontal length of $l_{a2} = 2.55\,\text{mm}$) is used to feed each rotational slot that has a narrow slot width of $w_s = 0.7\,\text{mm}$ and slot length $l_{s1} = 11.4\,\text{mm}$. It is also

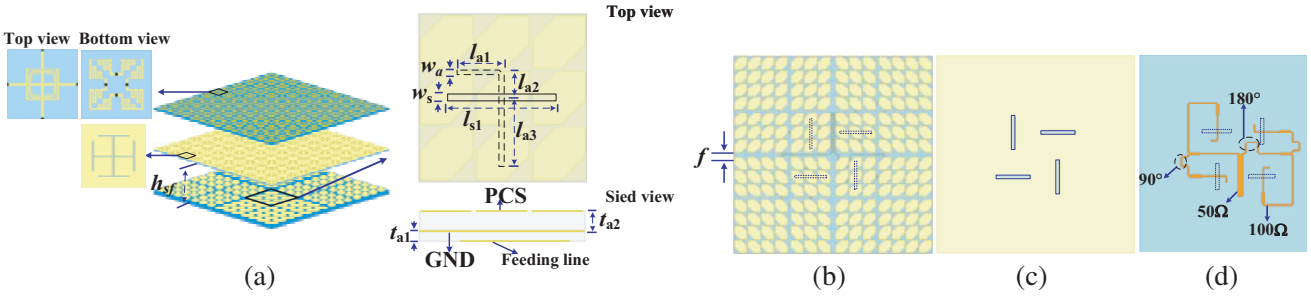

Figure 8. Schematic diagram of the CP slot antenna array loaded with FSR and PCS. (a) Overview. (b) Planar surface of the PCS (with the rotational slots beneath it). (c) Four (or 2×2) rotational slots loaded in the ground plane. (d) Sequential rotational feeding network for achieving right-hand CP. $h_{fs} = 4f = 2$, $l_{a1} = 4$, $l_{a2} = 2.55$, $l_{a3} = 7.25$, $l_{s1} = 11.4$, $w_a = 0.5$, $w_s = 0.7$, $t_{a1} = 0.787$, $t_{a2} = 1.575$. Unit: mm.

noteworthy that the four (or 2×2) narrow rotational slots are loaded directly beneath the PCS with a substrate thickness of $t_{a2} = 1.575\,\text{mm}$. The top view of the entire PCS (14×14 array type) that has the four narrow rotational slots located beneath it is shown in Fig. 8(b). Here, the entire PCS structure is composed of four major sets of 7×7 arrays, in which the two diagonal sets (at upper left and bottom right) have applied the Type 2 design (see Fig. 6(b)), and the other two diagonal sets (at upper right and bottom left) have applied the Type 1 design (see Fig. 6(a)). As for the small intervals (with width $f = 2\,\text{mm}$) that slightly separate these four major 7×7 array sets, they are for reducing the mutual coupling between the array units. Nevertheless, the main reason for the above PCS design is to achieve good phase cancellation, as well as enhancing the CP performance. Fig. 8(c) shows the planar surface of the four rotational slots loaded into the ground plane, which is located directly beneath the PCS (see Fig. 8(b)). The sequential rotational feeding network design is depicted in Fig. 8(d). It is printed on a Rogers substrate of thickness $t_{a1} = 0.787\,\text{mm}$, and it is directly stacked by the PCS, as shown in Fig. 8(a). By further observing Fig. 8(d), one can see that the sequential rotational (with phases 0°, 90°, 180°, and 270°) feeding lines are coupled-fed to the four rotational slots, which in turns excite a right-hand CP wave.

In order to verify the proposed design, the model depicted in Fig. 8 was fabricated separately and assembled. The top surface structure and bottom surface structure of the actual fabricated prototype of the FSA (11×11 units) are shown in Figs. 9(a) and 9(b), respectively. Fig. 9(c) shows the fabricated FSS (11×11 units), and Fig. 9(d) presents the fabricated PCS (14×14 units). As for the CP slot array, Fig. 9(e) shows the four rotational slots loaded on the ground plane printed on one side of the substrate, and Fig. 9(f) depicts the sequential rotational feeding network printed on the other side. Finally, all the above prototypes are assembled, and the final assembled prototype structure diagram is shown in Fig. 9(g).

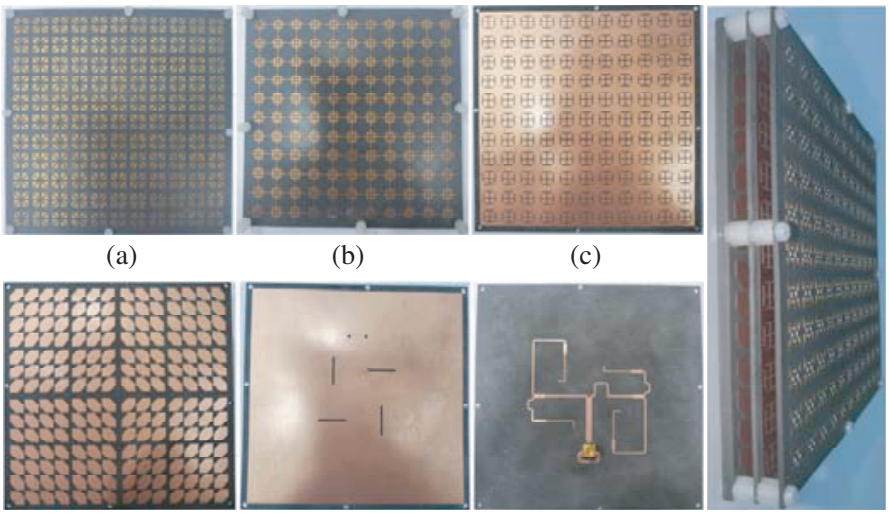

Figure 9. Fabricated prototype. (a) Front view of FSA. (b) Bottom view of FSA. (c) Front view of FSS. (d) Front view of PCS. (e) Ground plane with rotational slots. (f) Sequential rotational feeding network. (g) The final assembled prototype structure (CP slot antenna loaded with the FSR and PCS).

Figure 10 shows the simulated and measured results of the CP slot array loaded with only the PCS (without the FSR), and the two results are well-validated with each other. Notably, slight differences between the simulated and measured results are due to minor fabrication errors. In this figure, good 10-dB impedance bandwidth of approximately 15.5% (11.3–13.2 GHz) was measured, and its simulated one was 14.8% (11.3–13.1 GHz). By observing its corresponding axial ratio (AR) curve, one can see that the measured 3-dB AR bandwidth (or CP bandwidth) of the CP slot array was 11.4% (11.42–12.8 GHz), while its simulated one was 13.4% (11.26–12.88 GHz).

Figure 11 shows the simulated and measured results of the CP slot array loaded with both the

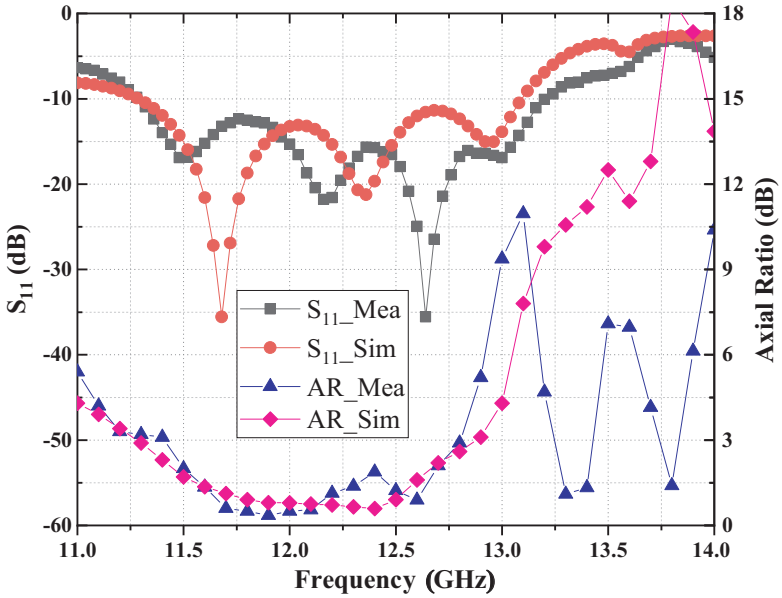

Figure 10. Measured and simulated reflection coefficient (S_{11}) and axial ratio (AR) of the proposed CP slot array loaded with PCS only (without FSR).

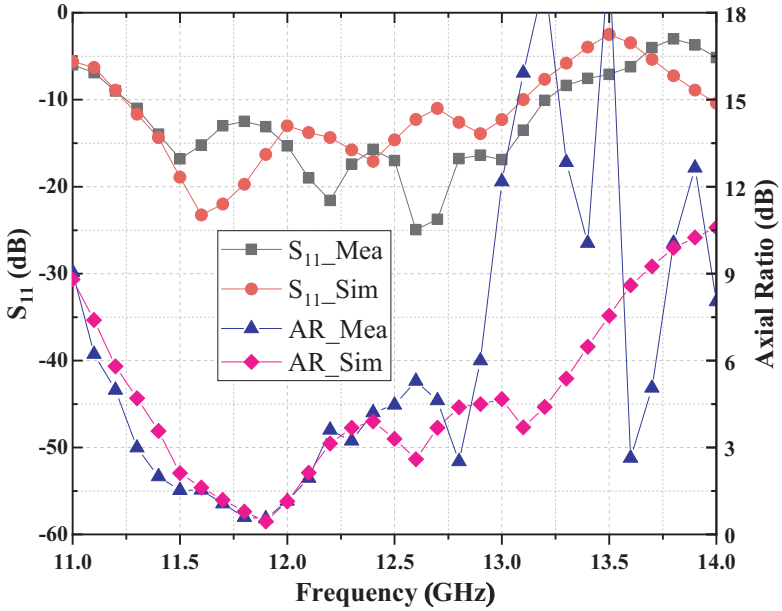

Figure 11. Measured and simulated reflection coefficient (S_{11}) and axial ratio (AR) of the proposed CP slot array loaded with PCS and FSR.

PCS and FSR structures. As depicted in Fig. 11, good 10-dB impedance bandwidth of 15.9% (11.25–13.2 GHz) was measured, and its corresponding simulated one was 15.3% (11.24–13.1 GHz). The measured 3-dB AR bandwidth of the CP slot array was 7.2% (11.3–12.15 GHz), and its simulated one was 5.9% (11.45–12.15 GHz). By further observing the results in Fig. 4 and Fig. 11, the effective bandwidth (or effective in-band) of the proposed CP slot antenna array loaded with FSR and PCS is 11.8–12.08 GHz.

The measured and simulated radiation patterns of the proposed (PCS loaded) CP slot antenna

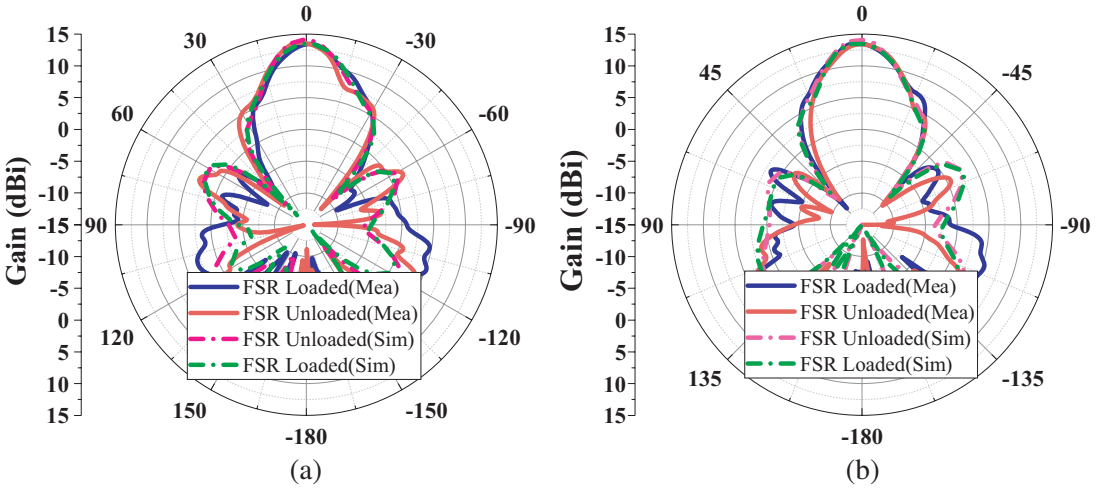

Figure 12. Measured and simulated radiation patterns of the proposed (PCS loaded) CP slot antenna array with and without loading the FSR at 11.9 GHz. (a) phi = 0°. (b) phi = 90°.

array with and without loading the FSR at 11.9 GHz rotated with two different phi angles, 0° and 90°, are plotted in Figs. 12(a) and 12(b), respectively. Here, one can see that the main beam of the (PCS loaded) CP slot array (with and without loading the FSR) can still exhibit similar main beam amplitude and beamwidth when the antenna is rotated from 0° to 90° (phi angle), meaning that the (PCS loaded) proposed CP slot array has very good CP performance. This phenomenon can be further comprehended by observing Figs. 10 and 11, in which the frequency at 11.9 GHz has a very low measured AR level of approximately 0.4. By further observing Fig. 12, the simulated peak gain of the (PCS loaded) CP slot antenna array (without loading the FSR) was 14 dBi, while its measured counterpart was only slightly lower at 13.6 dBi. In comparison, the measured peak gain of the (PCS loaded) CP slot antenna array (with loading the FSR) was 13.4 dBi, which has a difference of only 0.2 dB. Thus, one can conclude that the loading of FSR onto the proposed (PCS loaded) CP slot antenna array only results in a gain loss of

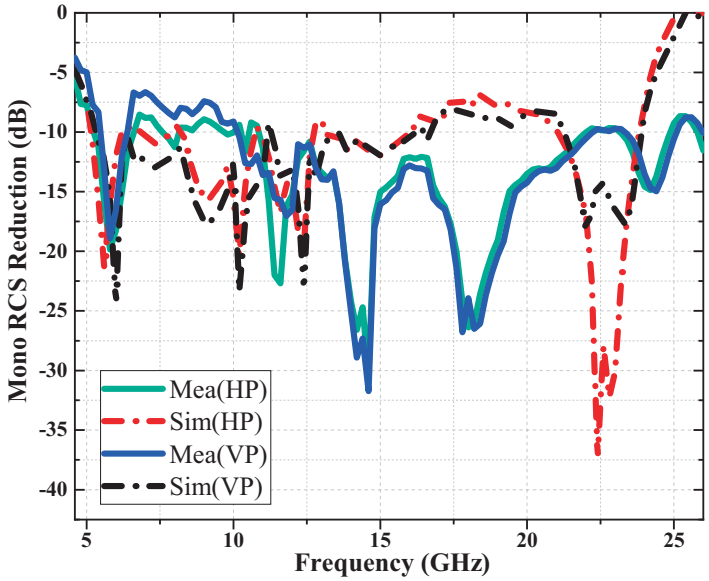

Figure 13. Measured and simulated monostatic RCS reduction of proposed CP slot antenna array loaded with FSR and PCS.

0.2 dB. Notably, this low gain losses phenomenon can be verified by the results shown in Fig. 4, in which the FSR has demonstrated an insertion loss of less than 0.3 dB across the passband (11.8–12.08 GHz). As the (PCS loaded) slot antenna array is exciting CP wave, this shows that the FSR proposed in the paper can also be applied to a radome with a multi-polarized antenna.

The measured and simulated monostatic RCS reductions of the proposed CP slot antenna array loaded with PCS and FRS are depicted in Fig. 13. Here, both the measured and simulated results show that the proposed method can achieve broadband monostatic RCS reduction for the CP slot antenna array, which can be established for both horizontal polarization (HP) and vertical polarization (VP). In this figure, it is noteworthy that the simulated RCS reduction range (greater than 7 dB) was approximately 5–24 GHz, but the measured RCS reduction range (greater than 7 dB) was approximately from 5 GHz to over 26 GHz. This phenomenon may be due to minor fabrication or assembling error that allows the higher resonances to shift to the higher spectrum (over 26 GHz). As our measurement equipment (anechoic chamber) can only measure up to a limit of 26 GHz, we can only yield an RCS reduction measurement of up to 26 GHz.

Table 1 shows the performances of the proposed work as compared with those that have been recently published. Here, one can see that the proposed method can achieve ultra-wideband reduction (with in-band and out-of-band RCS reduction range of 5–26 GHz greater than 7 dB), and the RCS reduction for the CP slot antenna array can be established for both horizontal polarization and vertical polarization EM waves.

Table 1. Performances comparison between the proposed work and other references.

Yr./Ref.	Ant. Pol. State	RCS Reduction BW, in % (GHz) (RCS Reduction threshold in dB)	RCS Reduction Pol. State
2020/[9]	CP	OB, 124% (2.0–4.77& 5.21–8.0) (NA)	HP
2020/[11]	LP	IB & OB, 100% (6.0–18.0) (NA)	HP and VP
2017/[20]	LP	IB & OB, 32.4% (2.85–3.95) ($>$ 4.3 dB)	HP and VP
2020/[21]	CP	IB & OB, 66.6% (5.0–10.0) ($>$ 4 dB)	HP and VP
2019/[22]	CP	IB & OB, 53.2% (5.1–8.8) (NA)	HP and VP
2017/[23]	CP	IB & OB, 38.6% (4.53–6.4) ($>$ 6 dB)	HP and VP
This Work	CP	IB and OB, 135.5% (5.0–26.0) ($>$ 7 dB)	HP and VP

Yr. $\sim$ Year, Ant. $\sim$ Antenna, Pol. $\sim$ Polarization, BW $\sim$ Bandwidth, OB $\sim$ Out-of-Band, IB $\sim$ In-Band, NA $\sim$ Not Available.

4. CONCLUSION

In this paper, a broadband monostatic RCS reduction of a CP slot antenna array was successfully investigated by loading a meticulously designed FSR and PCS onto a CP slot antenna array. Besides achieving a good RCS reduction range (greater than 7 dB) of approximately 5–26 GHz, it can also be established for both HP and VP incoming waves. Because the designed FSR has a low insertion loss of less than 0.3 dB across the passband (11.8–12.08 GHz), wide absorption band outside the passband of 4.7–10.7 GHz and 13.25–24.25 GHz (with absorption bandwidth of 136%), and high selectivity (Q factor value is 4.68), the effective in-band of the proposed CP slot antenna (loaded with the PCS and FSR) is 11.8–12.08 GHz, and it has a peak gain of 13.4 dBi at 11.9 GHz. In addition, the simulated and experimental results have also shown that the proposed FSR in this work can be applied to a radome with wide-beam and wide-angle scanning antennas, and when it is loaded on the CP antenna, the CP antenna pattern is not affected by it. As the proposed FSR is suitable for CP antenna radome and is conducive to the low-profile design of antennas and radomes, it has a much wider application prospect.

REFERENCES

1. Pang, Y. Q., Y. F. Li, B. Y. Qu, M. B. Yan, J. F. Wang, S. B. Qu, and Z. Xu, "Wideband RCS reduction metasurfacewith a transmission window," *IEEE Transactions on Antennas and Propagation*, Vol. 68, No. 10, 7079–7087, Oct. 2020.
2. Fan, Y., F. Wang, Y. F. Li, J. Q. Zhang, Y. J. Han, and B. Qu,"Low-RCS and high-gain circularly polarized metasurface antenna" *IEEE Transactions on Antennas and Propagation*, Vol. 67, No. 12, 7197–7203, Dec. 2019.
3. Paquay, M., J. Iriarte, I. Ederra, R. Gonzalo, and P. de Maagt, "Thin AMC structure for radar cross-section reduction," *IEEE Transactions on Antennas and Propagation*, Vol. 55, No. 12, 3630–3638, Dec. 2007.
4. Zheng, J., J. Gao, Y. L. Zho, X. Y. Cao, H. Yang, S. J. Li, and T. Li, "Wideband gain enhancement and RCS reduction of Fabr-Perot resonator antenna with chessboard arranged metamaterial superstrate"*IEEE Transactions on Antennas and Propagation*, Vol. 66, No. 2, 590–599, Feb. 2018.
5. Chen, W., C. A. Balanis, and C. R. Birtcher, "Checkerboard EBG surfaces for wideband radar cross section reduction" *IEEE Transactions on Antennas and Propagation*, Vol. 63, No. 6, 263–2645, Jun. 2015.
6. Samadi, F. and A. Sebak, "Wideband, very low RCS engineered surface with a wide incident angle stability," *IEEE Transactions on Antennas and Propagation*, Vol. 69, No. 3, 180–1814, Mar. 2021.
7. Su, J. X., Y. Lu, Y. Liu, Q. Yang, Z. R. Li, and J. M. Song, "A novel checker board metasurface based on optimized multielement phase cancellation for superwideband RCS reduction," *IEEE Transactions on Antennas and Propagation*, Vol. 66, No. 12, 709–7099, Dec. 2018.
8. Zheng, J., J. Gao, X. Y. Cao, D. Yuan, and H. H. Yang, "Wideband RCS reduction of a microstrip antenna using artificial magnetic conductor structures,"*IEEE Antennas and Wireless Propagation Letters*, Vol. 14, 158–1585, 2015.
9. Han, Y., L. Zhu, Y. M. Bo, W. Q. Che, and B. Li, "Novel low-RCS circularly polarized antenna arrays via frequency selective absorber," *IEEE Transactions on Antennas and Propagation*, Vol. 68, No. 1, 287–296, Jan. 2020.
10. Kundu, D., S. Baghel, A. Mohan, and A. Chakrabarty, "Design and analysis of printed lossy capacitive surface based ultrawideband low profile absorber," *IEEE Transactions on Antennas and Propagation*, Vol. 67, No. 5, 3533–3538, May 2019.
11. Liu, Y., Y. T. Jia, W. B. Zhang, and F. Li, "Wideband RCS reduction of a slot array antenna using a hybrid metasurface," *IEEE Transactions on Antennas and Propagation*, Vol. 68, No. 5, 364–3652, May 2020.
12. Costa, F. and A. Monorchio, "A frequency selective radom with wideband absorbing properties," *IEEE Transactions on Antennas and Propagation*, Vol. 60, No. 6, 274–2747, Jun. 2012.
13. Luo, G. Q., W. L. Yu, Y. F. Yu, H. Y. Jin, K. K. Fan, and F. Zhu, "Broadband dual-polarized band-absorptive frequency selective rasorber using absorptive transmission/reflection surface," *IEEE Transactions on Antennas and Propagation*, Vol. 68, No. 12, 7969–7977, Dec. 2020.
14. Ren, Y., W. Jiang, K. Z. Zhang, and X. Gong, "A high-gain circularly polarized Fabry-Perot antenna with wideband low-RCS property," *IEEE Antennas and Wireless Propagation Letters*, Vol. 17, No. 5, 85–856, May 2018.
15. Sang, D., Q. Chen, L. Ding, M. Guo, and Y. Q. Fu, "Design of checker board AMC structure for wideband RCS reduction," *IEEE Transactions on Antennas and Propagation*, Vol. 67, No. 4, 2604–2612, Apr. 2019.
16. Shang, Y. P., Z. X. Shen, and S. Q. Xiao, "Frequency-selective rasorber based on square-loop and crossdipole arrays," *IEEE Transactions on Antennas and Propagation*, Vol. 62, No. 11, 5581–5589, Nov. 2014.
17. Xia, J., F. Wei, T. Liu, L. Zhang, S. Guo, C. L. Li, S. W. Bie, and J. J. Jiang, "Design of a wideband absorption frequency selective rasorber based on double lossy layers," *IEEE Transactions on Antennas and Propagation*, Vol. 68, No. 7, 5718–5723, Jul. 2020.

18. Chen, Q., D. Sang, M. Guo, and Y. Q. Fu, "Frequency-selective rasorber with interabsorptionband transparent window and interdigital resonator," *IEEE Transactions on Antennas and Propagation*, Vol. 66, No. 8, 4105–4114, Aug. 2018.
19. Jia, Y., Y. Liu, Y. J. Guo, K. Li, and S. X. Gong, "A dual-patch polarization rotation reflective surface and its application to ultra-wideband RCS reduction," *IEEE Transactions on Antennas and Propagatio*, Vol. 65, No. 6, 3291–3295, Jun. 2017.
20. Han, Z. J., W. Song, and X. Q. Sheng, "Gain enhancement and RCS reduction for patch antenna by using polarization-dependent EBG surface," *IEEE Antennas and Wireless Propagation Letters*, Vol. 16, 1631–1634, Jan. 2017.
21. Pandit, S., A. Mohan, and P. Ray, "Low-RCS low-profile four-element MIMO antenna using polarization conversion metasurface," *IEEE Antennas and Wireless Propagation Letters*, Vol. 19, No. 12, 2102–2106, Dec. 2020.
22. Zhang, W., Y. Liu, and Y. Jia, "Circularly polarized antenna array with low RCS using metasurface-inspired antenna units," *IEEE Antennas and Wireless Propagation Letters*, Vol. 18, No. 7, 1453–1457, Jul. 2019.
23. Zhao, Y., X. Cao, J. Gao, L. Xu, X. Liu, and L. Cong, "Broadband low-RCS circularly polarized array using metasurface-based element," *IEEE Antennas and Wireless Propagation Letters*, Vol. 16, 1836–1839, 2017.